Realization of two-dimensional Aubry-André localization of light waves via electromagnetically induced transparency

Hui-jun Li,[1,2] Jian-peng Dou,[1] and Guoxiang Huang[2]

[1]*Institute of Nonlinear Physics and Department of Physics, Zhejiang Normal University, Jinhua, 321004 Zhejiang, China*

[2]*State Key Laboratory of Precision Spectroscopy and Department of Physics, East China Normal University, 200062 Shanghai, China*

(Received 6 November 2013; revised manuscript received 7 February 2014; published 24 March 2014)

We propose a scheme to construct a two-dimensional Aubry-André (AA) model and realize two-dimensional AA localization of light waves via electromagnetically induced transparency (EIT). The system we suggest is a cold, resonant atomic gas with an N-type level configuration and interacting with probe, control, assisted, and far-detuned laser fields. We show that under EIT conditions the probe-field envelope obeys a modified nonlinear Schrödinger equation with a quasiperiodic potential, which becomes a two-dimensional nonlinear AA model when the system parameters are suitably chosen. The quasiperiodic potential is obtained by the cross-phase modulation of the assisted field and the Stark shift of the far-detuned laser field. In addition, the cubic nonlinearity term appearing in the model is contributed by the self-phase modulation of the probe field. We demonstrate that the system can be used to not only realize various two-dimensional AA localizations of light waves, but also to display nonlinearity and dimensionality effects on the AA localizations.

DOI: 10.1103/PhysRevA.89.033843 PACS number(s): 42.25.Dd, 42.50.Gy, 42.65.Hw, 72.15.Rn

I. INTRODUCTION

Great interest in a wide class of quantum transport systems with periodic and disordered potentials has been triggered by the development of condensed matter physics. One of the most intriguing phenomena is the localization of particles and waves, called Anderson localization (AL) [1]. AL is important for the study of superconductors [2,3], Bose gases [4], and the phase transition of interacting fermions with a disorder potential [5], and so on. However, due to high electron-electron and electron-phonon interactions, up to now AL for noninteracting electrons has yet to be directly observed in solid-state materials.

Because AL may occur in any wave system with disorder, in recent years various setups where interaction or nonlinearity is nearly absent have attracted much attention. As a matter of course, sound and light waves [6–14], ultracold Bose and Fermi gases [4,5,15–21], etc., have been selected to be explored. Note that not only random disorder but also quasiperiodic systems can be used to study wave localizations. There are some differences between the wave localizations resulting respectively from random disorder and from quasiperiodic potentials. For instance, a transition from extended to localized states in a one-dimensional (1D) Aubry-André (AA) model [22] (also called the Harper model [23]) may occur, i.e., wave localization is possible in 1D for a quasiperiodic system. For convenience, in the following we call the localization resulting from quasiperiodic potentials as AA localization. However, if the potential is the one with random disorder, wave localization with the transition from extended to localized states occurs only for systems of more than two dimensions (2D).

In recent years, AA localization has become a topic of focus, and has been realized by using photonic lattices [13] and Bose-Einstein condensates [15]. Moreover, the effect of interaction on wave localization has also been studied in the AA model, but the conclusions obtained are still ambiguous. Reference [11] shows that self-focusing nonlinearity can result in a slight increase of the width of the localized wave packet, and Ref. [18] demonstrates that a repulsive interaction (equivalent to self-defocusing nonlinearity) may induce wave delocalization. The interplay between disorder and interaction is still an open question.

Though some means exist for adjusting the disorder potential and interparticle interaction, an active control of the disorder potential and interaction is desirable for practical applications. However, in active optical media, optical absorption is usually significant. In recent years, such a paradigm has been changed by the discovery of electromagnetically induced transparency (EIT). Due to the quantum interference effect induced by a control field, the optical absorption of the probe field in resonant atomic systems can be largely suppressed. Furthermore, EIT systems possess many striking features, including a large reduction of group velocity, a giant enhancement of Kerr nonlinearity, etc. [24]. Recently, Cheng and Huang have proposed a scheme to realize 1D AA localization via EIT [25].

In this article, we propose a scheme to construct a 2D AA model and realize 2D AA localization of light waves via EIT. The system we consider is a cold, resonant atomic gas having an N-type level configuration and interacting with probe, control, assisted, and far-detuned laser fields. We show that under EIT conditions the envelope of the probe field satisfies a modified (2+1)D nonlinear Schrödinger (NLS) equation with a quasiperiodic potential, which can be designed to be a 2D nonlinear AA model when the system parameters are suitably chosen. The quasiperiodic potential is obtained by the cross-phase modulation (CPM) of the assisted field and by the Stark shift of the far-detuned laser field. Additionally, the cubic nonlinearity term appearing in the model is contributed by the self-phase modulation (SPM) of the probe field. We demonstrate that the system can be used to not only realize various 2D AA localizations of light waves, but also to display the influence of nonlinearity and dimensionality effects on the AA localization.

The article is arranged as follows. In the next section, we describe the system under study. In Sec. III, using a method of multiple scales, we derive the modified NLS equation for the envelope of the probe field. In Sec. IV, we design various

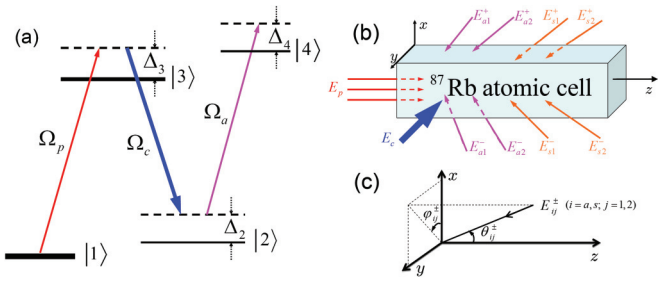

FIG. 1. (Color online) (a) Energy-level diagram and excitation scheme for the realization of the AA model. $|l\rangle$ ($l = 1,2,3,4$) are energy levels and Δ_3, Δ_2, and Δ_4 are one-, two-, and three-photon detunings, respectively. Ω_p, Ω_c, and Ω_a are half Rabi frequencies of the probe, control, and assisted laser fields, respectively. (b) Possible experimental arrangement of the laser fields, where E_p, E_c, E_a, and E_s are probe, control, assisted, and far-detuned laser fields, respectively. (c) Angles between the incident directions of the assisted field E_a and the far-detuned laser field E_s relative to the coordinate axes x, y, and z.

AA models and demonstrate various AA localizations in 2D, including the influence of nonlinearity and dimensionality. In the final section, we summarize the main results obtained in this work.

II. MODEL

We consider a cold, lifetime-broadened atomic gas with an N-type level configuration [Fig. 1(a)]. The levels are taken from the D_1 line of ^{87}Rb atoms, with $|1\rangle = |5S_{1/2}, F = 1\rangle$, $|2\rangle = |5S_{1/2}, F = 2\rangle$, $|3\rangle = |5P_{1/2}, F = 1\rangle$, and $|4\rangle = |5P_{1/2}, F = 2\rangle$. A weak probe field $\mathbf{E}_p = \mathbf{e}_p\mathcal{E}_p(x,y,z)\exp[i(k_pz - \omega_pt)] + \text{c.c.}$ and a strong control field $\mathbf{E}_c = \mathbf{e}_c\mathcal{E}_c\exp[i(-k_cy - \omega_ct)] + \text{c.c.}$ interact resonantly with levels $|1\rangle \to |3\rangle$ and $|2\rangle \to |3\rangle$, respectively. Here $\mathbf{e}_j$ and k_j ($\mathcal{E}_j$) are respectively the polarization unit vector in the jth direction and the wave number (envelope) of the jth field. The levels $|l\rangle$ ($l = 1,2,3$), together with $\mathbf{E}_p$ and $\mathbf{E}_c$, constitute a well-known Λ-type EIT core.

Furthermore, we assume the assisted field $\mathbf{E}_a$ with the form

$$\begin{aligned}\mathbf{E}_a &= \mathbf{e}_aE_a\exp(-i\omega_at) + \text{c.c.}\\ &= \mathbf{e}_a\frac{1}{2}(E_{a1}^+ + E_{a1}^- + E_{a2}^+ + E_{a2}^-)\exp(-i\omega_at) + \text{c.c.}\end{aligned} \quad (1)$$

is coupled to the levels $|2\rangle \to |4\rangle$, where $E_{aj}^\pm = \mathcal{E}_{aj}\exp[ik_a(\sin\theta_{aj}^\pm\cos\varphi_{aj}^\pm x + \sin\theta_{aj}^\pm\sin\varphi_{aj}^\pm y - \cos\theta_{aj}^\pm z) + i\psi_{aj}^\pm]$ ($j = 1,2$) [Fig. 1(b)], with $\theta_{ai}^\pm$ and $\varphi_{ai}^\pm$ shown in Fig. 1(c) and $\psi_{ai}^\pm$ the phase of the jth component of the assisted field. The assisted field $\mathbf{E}_a$, when assumed to be weak (satisfying $\mathcal{E}_p \sim E_a \ll \mathcal{E}_c$), will contribute a CPM effect to the probe field $\mathbf{E}_p$. Note that the levels $|l\rangle$ ($l = 1,2,3,4$), together with $\mathbf{E}_p$, $\mathbf{E}_c$, and $\mathbf{E}_a$, form an N-type system, which was considered first by Schmidt and Imamolu [26] for obtaining giant CPM via EIT.

In addition, we assume that another far-detuned (Stark) optical lattice field,

$$\begin{aligned}\mathbf{E}_{\text{Stark}} &= \mathbf{e}_s\sqrt{2}E_s\cos(\omega_st)\\ &= \mathbf{e}_s\frac{1}{\sqrt{2}}(E_{s1}^+ + E_{s1}^- + E_{s2}^+ + E_{s2}^-)\cos(\omega_st),\end{aligned} \quad (2)$$

is applied to the system. Here ω_s is the angular frequency and $E_{sj}^\pm = \mathcal{E}_{sj}\exp[ik_s(\sin\theta_{sj}^\pm\cos\varphi_{sj}^\pm x + \sin\theta_{sj}^\pm\sin\varphi_{sj}^\pm y - \cos\theta_{sj}^\pm z) + i\psi_{sj}^\pm]$ ($j = 1,2$), with $\theta_{sj}^\pm$ and $\varphi_{sj}^\pm$ shown in Fig. 1(c) and $\psi_{si}^\pm$ the phase of the jth component of the Stark field. Due to the existence of $\mathbf{E}_{\text{Stark}}$, a small but space-dependent Stark level shift $\Delta E_l = -\frac{1}{2}\alpha_l\langle\mathbf{E}_{\text{Stark}}^2\rangle_t = -\frac{1}{2}\alpha_l|E_s|^2$ occurs, where α_l is the scalar polarizability of the level $|l\rangle$, and $\langle\cdots\rangle$ denotes the time average in an oscillating cycle. The explicit forms of E_a and E_s in (1) and (2) will be chosen later on according to the requirement of the quasiperiodic potential (see Sec. IV A). As will be shown below, the CPM effect contributed by the assisted field $\mathbf{E}_a$ given by (1) and the Stark shift contributed by the far-detuned Stark field $\mathbf{E}_{\text{Stark}}$ given by (2) will provide the quasiperiodic refractive index to the evolution of the probe-field envelope.

Under the electric-dipole and rotating-wave approximations, the Hamiltonian of the system in the interaction picture reads

$$\begin{aligned}\hat{H}_{\text{int}} = &-\hbar\sum_{l=1}^{4}\Delta_l'|l\rangle\langle l| - \hbar(\Omega_p|3\rangle\langle 1| + \Omega_c|3\rangle\\ &\times\langle 2| + \Omega_a|4\rangle\langle 2| + \text{H.c.}),\end{aligned} \quad (3)$$

with $\Delta_l' = \Delta_l + [\alpha_l/(2\hbar)]|E_s|^2$, where $\Omega_p = (\mathbf{e}_p\cdot\mathbf{p}_{13})\mathcal{E}_p/\hbar$, $\Omega_c = (\mathbf{e}_c\cdot\mathbf{p}_{23})\mathcal{E}_c/\hbar$, and $\Omega_a = (\mathbf{e}_a\cdot\mathbf{p}_{24})E_a/\hbar$ are respectively the half Rabi frequencies of the probe, control, and assisted fields, with $\mathbf{p}_{jl}$ the electric-dipole matrix element related to the transition from $|j\rangle$ to $|l\rangle$; Δ_3, Δ_2, and Δ_4 are one-, two-, and three-photon detunings in the relevant transitions, respectively.

The motion of atoms is governed by the Bloch equation

$$\frac{\partial\sigma}{\partial t} = -\frac{i}{\hbar}[\hat{H}_{\text{int}},\sigma] - \Gamma\sigma, \quad (4)$$

where σ is a 4×4 density matrix in the interaction picture, and Γ is a 4×4 relaxation matrix describing the spontaneous emission and dephasing of the system. Explicit expressions of Eq. (4) are presented in the Appendix.

Under a slowly varying envelope approximation, the Maxwell equation of the probe field is reduced to [27]

$$i\frac{\partial\Omega_p}{\partial z} + \frac{c}{2\omega_p}\left(\frac{\partial^2}{\partial x^2} + \frac{\partial^2}{\partial y^2}\right)\Omega_p + \kappa_{13}\sigma_{31} = 0, \quad (5)$$

where $\kappa_{13} = N_a\omega_p|\mathbf{e}_p\cdot\mathbf{p}_{13}|^2/(2\epsilon_0\hbar c)$, with N_a the atomic concentration. Note that the dynamics of Ω_a is negligible during the probe-field evolution because the assisted field couples with the levels $|2\rangle$ and $|4\rangle$, which have a vanishing population due to the EIT induced by the strong control field.

III. ASYMPTOTIC EXPANSION AND MODIFIED (2+1)D NLS EQUATION

We employ the standard method of multiple scales [27] to investigate the evolution of the probe field. We make the asymptotic expansion $\sigma_{ij} = \epsilon\sigma_{ij}^{(1)} + \epsilon^3\sigma_{ij}^{(3)} + \cdots$ ($ij = 21,31$), $\sigma_{kl} = \sigma_{kl}^{(0)} + \epsilon^2\sigma_{kl}^{(1)} + \epsilon^3\sigma_{kl}^{(3)} + \cdots$ ($kl \neq ij$) (with $\sigma_{kl}^{(0)} = \delta_{k1}\delta_{l1}$), $\Omega_p = \epsilon\Omega_p^{(1)} + \epsilon^3\Omega_p^{(3)} + \cdots$, $\Omega_a = \epsilon\Omega_a^{(1)}$, $E_s = \epsilon E_s^{(1)}$, $d_{ij} = d_{ij}^{(0)} + \epsilon^2 d_{ij}^{(2)}$ (with $d_{ij}^{(0)} = \Delta_i - \Delta_j + i\gamma_{ij}$ and $d_{ij}^{(2)} = \frac{\alpha_i - \alpha_j}{2\hbar}|E_s^{(1)}|^2$). Here ϵ is a small parameter characterizing

the typical amplitude of the probe and the assisted fields. All quantities on the right-hand sides of the asymptotic expansion are considered as functions of the multiple scale variables $z_l = \epsilon^l z$ $(l = 0,2)$, $x_1 = \epsilon x$, and $y_1 = \epsilon y$. Substituting the expansion into Eqs. (A1) and (5), one can obtain a series of linear but inhomogeneous equations for $\sigma_{ij}^{(l)}$ and $\Omega_p^{(l)}$ $(l = 1,2,3,\ldots)$, which can be solved order by order.

At ϵ order, we obtain the linear solution

$$\Omega_p^{(1)} = Fe^{iKz_0} = Fe^{i\theta}, \tag{6a}$$

$$\sigma_{31}^{(1)} = \frac{d_{21}^{(0)}}{D}Fe^{i\theta}, \tag{6b}$$

$$\sigma_{21}^{(1)} = -\frac{\Omega_c^*}{D}Fe^{i\theta}, \tag{6c}$$

with $D = |\Omega_c|^2 - d_{21}^{(0)}d_{31}^{(0)}$. In above expressions, $K = \kappa_{13}d_{21}^{(0)}/D$ and F is to be the determined envelope function.

At ϵ^3 order, using the solvability condition for $\Omega_p^{(3)}$, we obtain the (2+1)D NLS equation

$$i\frac{\partial F}{\partial z_2} + \frac{c}{2\omega_p}\left(\frac{\partial^2}{\partial x_1^2} + \frac{\partial^2}{\partial y_1^2}\right)F + \alpha_{11}|F|^2F + \alpha_{12}\left|\Omega_a^{(1)}\right|^2F + \alpha_{13}\left|E_s^{(1)}\right|^2F = 0, \tag{7}$$

where

$$\alpha_{11} = -\frac{\kappa_{13}}{D}\left[6\frac{d_{21}^{(0)}}{\Gamma_{13}} + \frac{\Gamma_{23}}{\Gamma_{13}}\left(\frac{d_{32}^{(0)}}{\gamma_{32}} + \frac{d_{21}^{(0)}}{\gamma_{32}}\left|\frac{d_{32}^{(0)}}{\Omega_c}\right|^2\right)\right]\mathrm{Im}\left(\frac{d_{21}^{(0)}}{D}\right) - \frac{\kappa_{13}}{D}\left[\frac{|\Omega_c|^2}{\gamma_{32}}\mathrm{Im}\left(\frac{1}{D}\right) + \frac{d_{21}^{(0)}}{\gamma_{32}}\mathrm{Im}\left(\frac{d_{32}^{(0)}}{D}\right)\right], \tag{8a}$$

$$\alpha_{12} = -\frac{\kappa_{13}}{d_{41}^{(0)}}\frac{|\Omega_c|^2}{D^2}, \tag{8b}$$

$$\alpha_{13} = \frac{\kappa_{13}(\alpha_3 - \alpha_1)}{2\hbar D^2}\left(d_{21}^{(0)}\right)^2. \tag{8c}$$

After returning to the original variables, the (2+1)D NLS equation (7) takes the dimensionless form

$$i\frac{\partial u}{\partial s} + \frac{1}{2}\left(\frac{\partial^2}{\partial\xi^2} + \frac{\partial^2}{\partial\eta^2}\right)u + V(\xi,\eta)u = 0, \tag{9}$$

with

$$V(\xi,\eta) = V_{\mathrm{ex}}(\xi,\eta) + V_{\mathrm{int}}(\xi,\eta), \tag{10a}$$

$$V_{\mathrm{ex}}(\xi,\eta) = g_{12}c_v|v|^2 + g_{13}c_w|w|^2, \tag{10b}$$

$$V_{\mathrm{int}}(\xi,\eta) = g_{11}|u|^2, \tag{10c}$$

where $u = \Omega_p/U_0$, $v = \Omega_a/(\sqrt{c_v}V_0)$, $w = E_s/(\sqrt{c_w}E_{s0})$, $s = z/L_{\mathrm{diff}}$, $(\xi,\eta) = (x,y)/R_\perp$, $g_{11} = \alpha_{11}U_0^2/|\alpha_{13}E_{s0}^2|$, $g_{12} = \alpha_{12}V_0^2/|\alpha_{13}E_{s0}^2|$, and $g_{13} = \alpha_{13}/|\alpha_{13}|$. Here $L_{\mathrm{diff}} \equiv \omega_p R_\perp^2/c$ is the typical diffraction length ($R_\perp$ is the typical transverse beam radius). We have taken $L_{\mathrm{diff}} = L_{\mathrm{NL}}$ [$L_{\mathrm{NL}} = 1/(|\alpha_{13}E_{s0}^2|)$ is the typical nonlinearity length], which yields $E_{s0} = \sqrt{c/(\omega_p R_\perp^2|\alpha_{13}|)}$. Note that U_0 and V_0 are respectively typical Rabi frequencies of the probe and assisted fields, E_{s0} is the typical amplitude of the far-detuning laser field, and all of these parameters can be used to adjust the potential $V(\xi,\eta)$.

Obviously, the potential $V(\xi,\eta)$ given in expression (10a) includes the external potential (10b) contributed by the CPM effect from the assisted and far-detuned laser fields, and the nonlinear potential (10c) contributed by the SPM effect from the probe field. From the coefficients $\alpha_{11,12,13}$ given by expression (8), we see that the coefficients $g_{11,12,13}$ are controlled by U_0, V_0, E_{s0}, $\Delta_{2,3,4}$, and the intensity of the control field.

Note that under the EIT condition $|\Omega_c|^2 \gg \gamma_3\gamma_2$, the absorption of the probe field is largely suppressed, and hence the imaginary parts of the complex coefficients in Eq. (9) are relatively small (see the numerical examples given below).

IV. DESIGN OF THE 2D AA MODEL AND REALIZATION OF 2D AA LOCALIZATIONS

A. Design of the 2D AA model

To obtain a quasiperiodic potential required by the construction of a 2D AA model, we make an estimation of the numerical values of the coefficients in Eq. (9). We consider a typical cold atomic gas of ^{87}Rb atoms with D_1 line transitions $5^2S_{1/2} \to 5^2P_{1/2}$. The energy levels are chosen as those illustrated in Fig. 1(a). From the data of ^{87}Rb [28], system parameters can be chosen as $2\gamma_2 = 1 \times 10^3$ Hz, $\Gamma_{3,4} = 36$ MHz, $\kappa_{13} = 1.0 \times 10^{11}$ cm^{-1} s^{-1}, $\omega_p = 2.37 \times 10^{15}$ s^{-1}, $R_\perp = 3.6 \times 10^{-3}$ cm, $\Omega_c = 2.5 \times 10^7$ s^{-1}, $\Delta_2 = 0$ s^{-1}, $\Delta_4 = -\Delta_3 = 6.0 \times 10^8$ s^{-1}, $E_{s0} = 6.31 \times 10^6$ V cm^{-1}. Based on these parameters, we obtain $L_{\mathrm{diff}} = 1.0$ cm, $U_0 = 1.07 \times 10^7$ s^{-1}, and $V_0 = 1.92 \times 10^6$ s^{-1}. Thus we have

$$g_{11} = 1.0 - 0.03i, \quad g_{12} = -1.0 + i0.03, \quad g_{13} = -1.0 + 0.001i. \tag{11}$$

Since $\mathrm{Re}(g_{11})$ is positive, the system in this case has the property of self-focusing. If we take $\Delta_3 = 6.0 \times 10^8$ s^{-1}, we obtain

$$g_{11} = -1.0 - 0.03i, \quad g_{12} = -1.0 + i0.03, \quad g_{13} = -1.0 - 0.001i, \tag{12}$$

corresponding to a case of self-defocusing. In fact, the coefficients g_{jl} in Eq. (9) can be actively adjusted by choosing different system parameters, especially with different Δ_3, Δ_4, and E_{s0}. Thus the different 2D AA models can be realized in our system, as shown below.

From the results given by (11) and (12), we see that the imaginary parts of the coefficients in Eq. (9) are indeed much less than their real parts. The physical reason for such small imaginary parts is due to the EIT effect induced by the control field that makes the absorption of the probe field be largely suppressed. In the following, the small imaginary parts of these coefficients of g_{jl} will be neglected for simplicity.

By selecting different assisted and far-detuned laser fields, we can obtain many different V_{ex}, which are 2D quasiperiodic functions. Four of them are listed in the following:

Potential (1): By taking $\theta_{ai}^+ = -\theta_{ai}^- = \theta_{ai}$, $\varphi_{ai}^\pm = 0$, $\psi_{ai}^+ = -\psi_{ai}^- = -\pi/2$ $(i = 1,2)$, $\theta_{si}^+ = -\theta_{si}^- = \theta_{si}$, $\varphi_{si}^\pm = \pi/2$, $\psi_{si}^+ = -\psi_{si}^- = -\pi/2$ $(i = 1,2)$, $\cos\theta_j \approx 1$, and $\sin\theta_j \ll 1$ $(j = a1,a2,s1,s2)$, we obtain

$$E_a = \mathcal{E}_{a1}\left[\sin(x/R_\perp) + c_1\sin(\beta x/R_\perp)\right]\exp(-ik_a z), \tag{13a}$$

$$E_s = \mathcal{E}_{s1}\left[\sin(y/R_\perp) + c_1\sin(\beta y/R_\perp)\right]\exp(-ik_s z), \tag{13b}$$

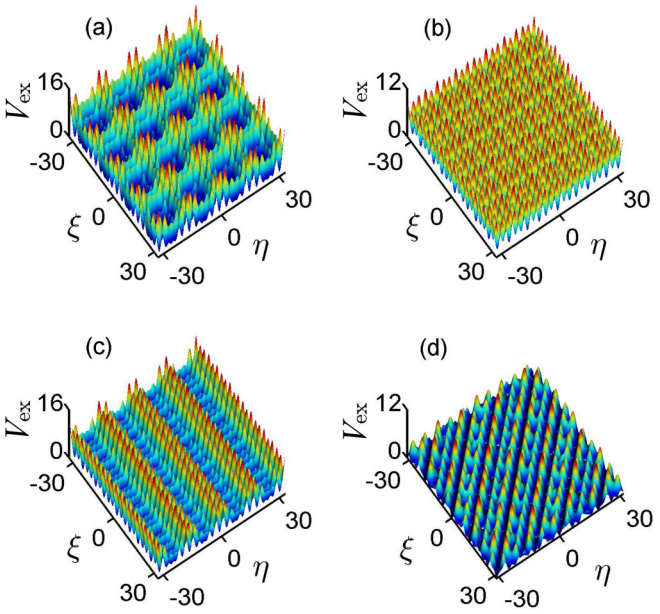

FIG. 2. (Color online) 3D surface plot of quasiperiodic potential V_{ex} as a function of ξ and η. (a) $V_{ex} = 2.724|\sin\xi + c_1\sin(\beta\xi)|^2 + 2.724|\sin\eta + c_1\sin(\beta\eta)|^2$. (b) $V_{ex} = 3[\sin^2\xi + c_1^2\sin^2(\beta\xi)] + 3[\sin^2\eta + c_1^2\sin^2(\beta\eta)]$. (c) $V_{ex} = 3[\sin^2\xi + c_1^2\sin^2(\beta\xi)] + 2.724|\sin\eta + c_1\sin(\beta\eta)|^2$. (d) $V_{ex} = c_1|\sin(\beta\xi) + \sin(\beta\eta)|^2 + |\sin\xi + \sin\eta|^2$. For all panels, $c_1 = 0.7$ and $\beta = \frac{\sqrt{5}-1}{2}$.

with $c_1 = \mathcal{E}_{a2}/\mathcal{E}_{a1} = \mathcal{E}_{s2}/\mathcal{E}_{s1}$, $\beta = \sin\theta_{a2}/\sin\theta_{a1} = \sin\theta_{s2}/\sin\theta_{s1}$, $R_\perp = (k_a\sin\theta_{a1})^{-1} = (k_s\sin\theta_{s1})^{-1}$. As a result, we have $|v|^2 = |\sin\xi + c_1\sin(\beta\xi)|^2$, $|w|^2 = |\sin\eta + c_1\sin(\beta\eta)|^2$, and hence

$$V_{ex}(\xi,\eta) = 2.724|\sin\xi + c_1\sin(\beta\xi)|^2 + 2.724|\sin\eta + c_1\sin(\beta\eta)|^2. \quad (14)$$

Shown in Fig. 2(a) is the three-dimensional (3D) surface plot of the potential V_{ex} as a function of ξ and η for $c_v = c_w = 2.724$, $c_1 = 0.7$, and $\beta = \frac{\sqrt{5}-1}{2}$. We see that around the middle point $(\xi,\eta) = (0,0)$ there are four nearest-neighbor potential traps, by which four localized peaks of $|u|$ will form (see Fig. 3 below). The potential is quasiperiodic but has a regular distribution.

Potential (2): By taking $\theta_{ai}^+ = -\theta_{ai}^- = \theta_{ai}$, $\varphi_{ai}^\pm = 0$ $(i = 1,2)$, $\psi_{a1}^+ = -\psi_{a1}^- = -\pi/2$, $\psi_{a2}^+ = 0$, $\psi_{a2}^- = \pi$, $\theta_{si}^+ = -\theta_{si}^- = \theta_{si}$, $\varphi_{si}^\pm = \pi/2$ $(i = 1,2)$, $\psi_{s1}^+ = -\psi_{s1}^- = -\pi/2$, $\psi_{s2}^+ = 0$, $\psi_{s2}^- = \pi$, $\cos\theta_j \approx 1$, and $\sin\theta_j \ll 1$ $(j = a1,a2,s1,s2)$, we get

$$E_a = \mathcal{E}_{a1}[\sin(x/R_\perp) + ic_1\sin(\beta x/R_\perp)]\exp(-ik_a z), \quad (15a)$$

$$E_s = \mathcal{E}_{s1}[\sin(y/R_\perp) + ic_1\sin(\beta y/R_\perp)]\exp(-ik_s z). \quad (15b)$$

Then one has $|v|^2 = [\sin^2\xi + c_1^2\sin^2(\beta\xi)]$, $|w|^2 = [\sin^2\eta + c_1^2\sin^2(\beta\eta)]$, and $\beta = \frac{\sqrt{5}-1}{2}$. Thus we obtain the quasiperiodic potential

$$V_{ex}(\xi,\eta) = 3\left[\sin^2\xi + c_1^2\sin^2(\beta\xi)\right] + 3\left[\sin^2\eta + c_1^2\sin^2(\beta\eta)\right] \quad (16)$$

for $c_v = c_w = 3$, $c_1 = 0.7$, and $\beta = \frac{\sqrt{5}-1}{2}$. Figure 2(b) shows V_{ex} as the function of ξ and η. The potential distribution looks homogeneous, but it is indeed quasiperiodic.

Potential (3): If we take $\theta_{ai}^+ = -\theta_{ai}^- = \theta_{ai}$, $\varphi_{ai}^\pm = 0$ $(i = 1,2)$, $\psi_{a1}^+ = -\psi_{a1}^- = -\pi/2$, $\psi_{a2}^+ = 0$, $\psi_{a2}^- = \pi$, $\theta_{si}^+ = -\theta_{si}^- = \theta_{si}$, $\varphi_{si}^\pm = \pi/2$ $\psi_{si}^+ = -\psi_{si}^- = -\pi/2$ $(i = 1,2)$, $\cos\theta_j \approx 1$, and $\sin\theta_j \ll 1$ $(j = a1,a2,s1,s2)$, we have

$$E_a = \mathcal{E}_{a1}[\sin(x/R_\perp) + ic_1\sin(\beta x/R_\perp)]\exp(-ik_a z), \quad (17a)$$

$$E_s = \mathcal{E}_{s1}[\sin(y/R_\perp) + c_1\sin(\beta y/R_\perp)]\exp(-ik_s z). \quad (17b)$$

In this case, $|v|^2 = [\sin^2\xi + c_1^2\sin^2(\beta\xi)]$, $|w|^2 = |\sin\eta + c_1\sin(\beta\eta)|^2$. As a result, we obtain the quasiperiodic potential

$$V_{ex}(\xi,\eta) = 3\left[\sin^2\xi + c_1^2\sin^2(\beta\xi)\right] + 2.724|\sin\eta + c_1\sin(\beta\eta)|^2 \quad (18)$$

for $c_v = 3$, $c_w = 2.724$, $c_1 = 0.7$, and $\beta = \frac{\sqrt{5}-1}{2}$. The corresponding 3D surface plot is illustrated in Fig. 2(c).

Potential (4): When taking $\theta_{ai}^+ = -\theta_{ai}^- = \theta_a$, $\varphi_{a1}^\pm = 0$, $\varphi_{a2}^\pm = \pi/2$, $\psi_{ai}^+ = \psi_0 - \pi/2, \psi_{ai}^- = \psi_0 + \pi/2 (i = 1,2)$, $\theta_{si}^+ = -\theta_{si}^- = \theta_s$, $\varphi_{s1}^\pm = 0$, $\varphi_{s2}^\pm = \pi/2$, $\psi_{si}^+ = -\psi_{si}^- = -\pi/2$ $(i = 1,2)$, $\cos\theta_j \approx 1$, and $\sin\theta_j \ll 1$ $(j = a1,a2,s1,s2)$, we get

$$E_a = \mathcal{E}_{a1}[\sin(\beta x/R_\perp) + \sin(\beta y/R_\perp)]\exp(-ik_a z), \quad (19a)$$

$$E_s = \mathcal{E}_{s1}[\sin(x/R_\perp) + \sin(y/R_\perp)]\exp(-ik_s z), \quad (19b)$$

where $\mathcal{E}_{a2}/\mathcal{E}_{a1} = \mathcal{E}_{s2}/\mathcal{E}_{s1} = 1$, $\beta = k_a\sin\theta_a/(k_s\sin\theta_s)$, $R_\perp = (k_s\sin\theta_s)^{-1}$. Thus we have $|v|^2 = |\sin(\beta\xi) + \sin(\beta\eta)|^2$, and $|w|^2 = |\sin\xi + \sin\eta|^2$. The quasiperiodic potential is given by

$$V_{ex}(\xi,\eta) = c_1|\sin(\beta\xi) + \sin(\beta\eta)|^2 + |\sin\xi + \sin\eta|^2 \quad (20)$$

for $c_v = c_1$, $c_w = 1$, and $\beta = \frac{\sqrt{5}-1}{2}$. The corresponding 3D surface plot is shown in Fig. 2(d).

Because the potentials given above are quasiperiodic, Eq. (9) with any of them is a 2D nonlinear AA model. Note that for all four potentials given above, the parameter c_1 is used to modulate the periodicity of V_{ex}. With an increase of c_1, V_{ex} is changed from periodic, to nearly periodic, and then to quasiperiodic. Of course, we can also choose different $\varphi_{a1,a2,s1,s2}^\pm$, $\theta_{a1,a2,s1,s2}^\pm$, and $\psi_{a1,a2,s1,s2}^\pm$ to construct some other types of quasiperiodic potentials, which are not listed here to save space.

B. Delocalization-localization transition in the 2D linear AA model

We now turn to investigate various 2D AA localizations of the system by using the 2D AA model obtained above. If the amplitude of the probe field is small, the nonlinear potential in Eq. (10a) (i.e., V_{int}) is negligible. In this situation, Eq. (9) is reduced to the 2D linear AA model

$$i\frac{\partial u}{\partial s} + \frac{1}{2}\left(\frac{\partial^2}{\partial\xi^2} + \frac{\partial^2}{\partial\eta^2}\right)u + V_{ex}(\xi,\eta)u = 0. \quad (21)$$

Figure 3 shows the absolute value of the ground-state wave function $|u|$ of Eq. (21) with different quasiperiodic potentials $V_{ex}(\xi,\eta)$. Figures 3(a)–3(c) illustrate the results of the first kind

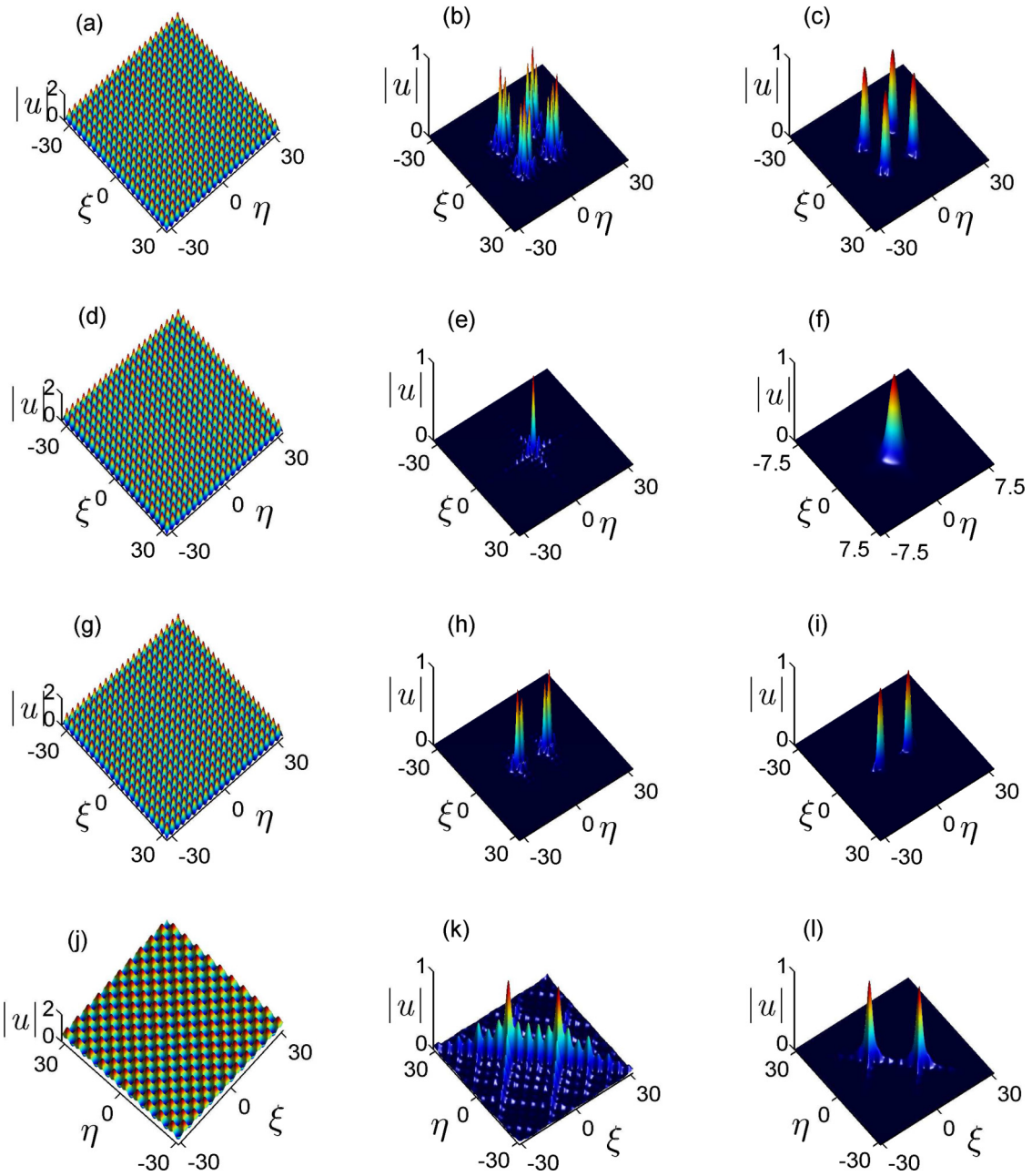

FIG. 3. (Color online) Delocalization-localization transition in the 2D linear AA model. (a)–(c) show the numerical results of $|u|$ for the ground state of Eq. (21) with the potential (14) when the modulation depth c_1 takes 0, 0.15, and 0.7, respectively. (d)–(f) show the numerical results of $|u|$ for the ground state of Eq. (21) with the potential (16) when c_1 takes 0, 0.25, and 0.7, respectively. (g)–(i) show the numerical results of $|u|$ for the ground state of Eq. (21) with the potential (18) when c_1 takes 0, 0.3, and 0.7, respectively. (j)–(l) show the numerical results of $|u|$ for the ground state of Eq. (21) with the potential (20) when c_1 takes values 0, 0.1, and 0.7, respectively.

of quasiperiodic potential (14) when the modulation strength c_1 takes different values. Figure 3(a) displays the result for $c_1 = 0$. Since the potential $V_{ex}(\xi,\eta)$ in this case is periodic, the ground state is a periodic extended state. Figure 3(b) shows the result for $c_1 = 0.15$. In this case $V_{ex}(\xi,\eta)$ is quasiperiodic, and four wave peaks appear near the center of the figure, i.e., the state begins to localize. Because each peak has a rugged structure and a large width, the localization is not complete. However, when c_1 is increased to 0.7 [Fig. 3(c)], a perfect 2D localization occurs. In this case, the four peaks become extremely smooth and have a very small width.

Illustrated in Figs. 3(d)–3(f) are the results of the second kind of quasiperiodic potential (16) when c_1 takes 0, 0.25, and 0.7, respectively. We see that the ground-state wave function $|u|$ displays a perfect transition from a periodic extended state to a localized state. In particular, in this situation only a single wave peak appears near $(\xi,\eta) = (0,0)$ in the localized state.

Illustrated in Figs. 3(g)–3(i) are the results of the third kind of quasiperiodic potential (18) for c_1 taking 0, 0.3, and 0.7, respectively. In this situation, the localized state has two wave peaks appearing along the η axis at $\xi = 0$. Shown in Figs. 3(j)–3(l) are the results of the fourth kind of quasiperiodic potential

(20) when c_1 takes 0, 0.1, and 0.7, respectively. Differently, here in the localized state, two large wave peaks appear along the diagonal direction of the (ξ,η) plane.

From Fig. 3 we see that for all four kinds of quasiperiodic potentials, the system displays an AA localization and undergoes a delocalization-localization transition when changing the modulation depth c_1. We stress that in our system such a delocalization-localization transition can be manipulated actively because c_1 depends on $\mathcal{E}_{a2}$, $\mathcal{E}_{a1}$, $\mathcal{E}_{s2}$, and $\mathcal{E}_{s1}$. That is to say, we can choose different amplitudes of the assisted field and the optical lattice field [see Eqs. (1) and (2)] to obtain different values of c_1, and hence to realize the delocalization-localization transition in a controllable way.

C. Effects of dimensionality and nonlinearity on the AA localization

1. *Dimensionality effect on the localization in the linear AA model*

In Refs. [13,25], AA localization in discrete and continuous 1D linear AA models has been clearly demonstrated. As shown above, the 2D linear AA model can also be used to realize AA localization. One may ask the question regarding the difference between 1D and 2D localizations in models with quasiperiodic potentials.

In order to illustrate the dimensionality effect and make a comparison of localizations between linear AA models in both 1D and 2D, we calculate the participation ratio (PR) defined by [13,25]

$$\mathrm{PR} = \frac{[\iint |u(\xi,\eta,s)|^2 d\xi d\eta]^2}{\iint |u(\xi,\eta,s)|^4 d\xi d\eta}, \tag{22}$$

which describes the width of the wave function $|u|$. For comparison, in addition to the 2D linear AA model given by Eq. (21), we also consider the 1D linear AA model of the form

$$i\frac{\partial u}{\partial s} + \frac{1}{2}\frac{\partial^2 u}{\partial \xi^2} + V_{\mathrm{ex}}(\xi)u = 0. \tag{23}$$

Note that such a model can be obtained for a probe beam having a large width in the y direction, i.e., the diffraction term $\partial^2 u/\partial\eta^2$ can be disregarded. In addition, the assisted and optical lattice fields are taken to be y independent and hence there is no η dependence in the quasiperiodic potential. In this situation, the 2D linear AA model Eq. (21) is converted into the 1D linear AA model (23). To save space here we only present the results for the first and second kinds of quasiperiodic potentials [i.e., (14) and (16)].

Shown in Fig. 4(a) is the result of PR_1 (normalized PR) as a function of c_1 for the 2D linear AA model (21) (blue dashed line) and the 1D linear AA model (23) (red solid line) with the quasiperiodic potential (14). The black dot in the figure indicates the transition point from delocalization (left) to localization (right). We see the following: (i) The transition points from delocalization to localization in the c_1 axis are almost the same for both the 1D and 2D AA models (i.e., $c_1 \approx 0.095$). (ii) The AA localization is more pronounced in 2D than in 1D because the value of PR_1 in 2D is smaller than that in 1D for all c_1.

Figure 4(b) shows the result of PR_1 as a function of c_1 for the 2D linear AA model (21) and the 1D linear AA model (23) with the quasiperiodic potential (16). One sees that a conclusion similar to that of Fig. 4(a) can be obtained. However, in this case the value of c_1 at the transition point is larger (around 0.2).

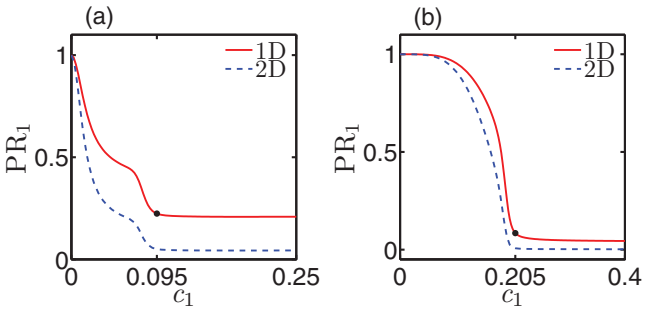

FIG. 4. (Color online) Dimensionality effect on the localization in linear AA models. (a) Normalized PR curve PR_1 as a function of modulation depth c_1 for the 2D linear AA model (21) (blue dashed line) and the 1D linear AA model (23) (red solid line) with the quasiperiodic potential (14). (b) Normalized PR curve PR_1 as a function of c_1 for the 2D linear AA model (21) and the 1D linear AA model (23) with the quasiperiodic potential (16). The black point in each panel indicates the transition point from delocalization (left) to localization (right).

2. *Nonlinear effect on the localization in the 2D AA model*

If the amplitude of the probe field is not small, the nonlinear effect of the system must be taken into account. In the situation of weak nonlinearity considered in the present work, the amplitude equation is given by the 2D nonlinear AA model (9) where the nonlinear potential V_{int} cannot be neglected. One can also ask the question regarding the effect of nonlinearity on the 2D AA localization.

In this section, we discuss the nonlinearity effect on the AA localization by numerically solving the 2D AA model (9) with the first kind of quasiperiodic potential (14).

Figures 5(a) and 5(b) show the results of the 2D nonlinear AA model (9) for the first kind of quasiperiodic potential (14) and for a propagation distance $s = 10$. Shown in Fig. 5(a)

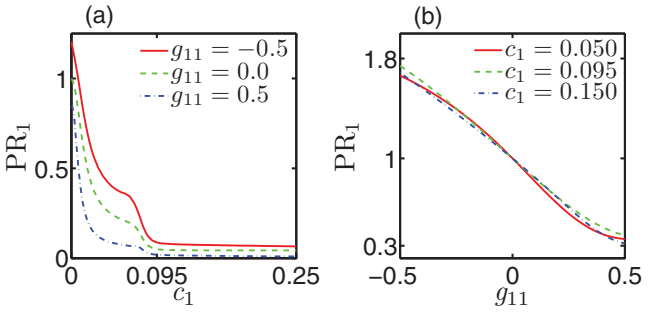

FIG. 5. (Color online) Nonlinear effect on the localization in the 2D AA model. (a) PR_1 curve as a function of the modulation depth c_1. The solid, dashed, and dotted-dashed lines are for $g_{11} = -0.5, 0, 0.5$, respectively. (b) PR_1 curve as a function of the nonlinear coefficient g_{11}. The solid, dashed, and dotted-dashed lines are for $c_1 = 0.050, 0.095, 0.150$, respectively. When obtaining the results in (a) and (b), the quasiperiodic potential (14) is used. All these PR_1 curves have been normalized by the maximum PR value for $g_{11} = 0$ in (a) and by PR values for $g_{11} = 0$ in (b).

is the PR_1 curve as a function of the modulation depth c_1. The solid, dashed, and dotted-dashed lines in the figure are for the nonlinear coefficients $g_{11} = -0.5, 0, 0.5$, respectively. Note that all these PR_1 curves have been normalized by the maximum PR value for $g_{11} = 0$ in (a) and by PR values for $g_{11} = 0$ in (b). We see that the nonlinearity (i.e., $g_{11} \neq 0$) indeed has an obvious effect on the localization property of the system. In particular, the self-focusing nonlinearity (i.e., $g_{11} > 0$) can enhance the AA localization, but the self-defocusing nonlinearity (i.e., $g_{11} < 0$) contributes a delocalization effect. Interestingly, the delocalization-localization transition points are nearly the same for different values of g_{11}.

Shown in Fig. 5(b) is the PR_1 curve as a function of the nonlinear coefficient g_{11}. The solid, dashed, and dotted-dashed lines are for $c_1 = 0.050, 0.095, 0.150$, respectively. This figure shows clearly that the AA localization in the self-focusing case ($g_{11} > 0$) is more pronounced than that in the self-defocusing case ($g_{11} < 0$) in spite of the value of c_1.

Based on the results obtained above, we have the following conclusions: (i) Dimensionality, nonlinearity, and the form of the quasiperiodic potential have effects on the AA localization. (ii) Generally, the system with a higher spatial dimensionality has more pronounced AA localization. (iii) Self-focusing nonlinearity can enhance the AA localization, but self-defocusing nonlinearity weakens the AA localization. We stress that the system we consider here not only provides a simple way of realizing 2D AA localization via EIT, which is quite different from off-resonant mechanisms, but also has the advantages of actively controlling the quasiperiodic potential, dimensionality, and nonlinearity, allowing easy manipulation of the delocalization-localization transition based on atomic coherence.

V. SUMMARY

In this article we have proposed a scheme to construct the 2D AA model and realize 2D AA localizations of light waves via EIT. The system we consider is a cold, resonant atomic gas having an N-type level configuration and interacting with probe, control, assisted, and far-detuned laser fields. We have shown that under EIT conditions the envelope of the probe field satisfies a modified NLS equation with a quasiperiodic potential, which can be designed to be a nonlinear 2D AA model when the system parameters are suitably chosen. The quasiperiodic potential is obtained by the CPM of the assisted field and the Stark shift of the far-detuned laser field. Additionally, the cubic nonlinearity term appearing in the model is contributed by the SPM of the probe field. We have demonstrated that the system can be used not only to realize various 2D AA localizations of light waves, but also to display the influence of nonlinearity and dimensionality effects on the AA localizations.

ACKNOWLEDGMENT

This work was supported by the NSF-China under Grants No. 11074221, No. 11174080, and No. 11204274, by the discipline construction funds of ZJNU under Grant No. ZC323007110, by the Doctoral Foundation of ZJNU 2009, and by the Open Fund from the State Key Laboratory of Precision Spectroscopy, ECNU.

APPENDIX: EQUATIONS OF MOTION FOR σ_{ij}

Equations of motion for σ_{ij} are given by

$$i\frac{\partial}{\partial t}\sigma_{11} - i\Gamma_{13}\sigma_{33} + \Omega_p^*\sigma_{31} - \Omega_p\sigma_{31}^* = 0, \tag{A1a}$$

$$i\frac{\partial}{\partial t}\sigma_{22} - i\Gamma_{23}\sigma_{33} - i\Gamma_{24}\sigma_{44} + \Omega_c^*\sigma_{32} - \Omega_c\sigma_{32}^* + \Omega_a^*\sigma_{42} - \Omega_a\sigma_{42}^* = 0, \tag{A1b}$$

$$i\left(\frac{\partial}{\partial t} + \Gamma_3\right)\sigma_{33} - \Omega_p^*\sigma_{31} + \Omega_p\sigma_{31}^* - \Omega_c^*\sigma_{32} + \Omega_c\sigma_{32}^* = 0, \tag{A1c}$$

$$i\left(\frac{\partial}{\partial t} + \Gamma_4\right)\sigma_{44} - \Omega_a^*\sigma_{42} + \Omega_a\sigma_{42}^* = 0, \tag{A1d}$$

$$\left(i\frac{\partial}{\partial t} + d_{21}\right)\sigma_{21} + \Omega_c^*\sigma_{31} + \Omega_a^*\sigma_{41} - \Omega_p\sigma_{32}^* = 0, \tag{A1e}$$

$$\left(i\frac{\partial}{\partial t} + d_{31}\right)\sigma_{31} + \Omega_p(\sigma_{11} - \sigma_{33}) + \Omega_c\sigma_{21} = 0, \tag{A1f}$$

$$\left(i\frac{\partial}{\partial t} + d_{41}\right)\sigma_{41} + \Omega_a\sigma_{21} - \Omega_p\sigma_{43} = 0, \tag{A1g}$$

$$\left(i\frac{\partial}{\partial t} + d_{32}\right)\sigma_{32} + \Omega_c(\sigma_{22} - \sigma_{33}) + \Omega_p\sigma_{21}^* - \Omega_a\sigma_{43}^* = 0, \tag{A1h}$$

$$\left(i\frac{\partial}{\partial t} + d_{42}\right)\sigma_{42} + \Omega_a(\sigma_{22} - \sigma_{44}) - \Omega_c\sigma_{43} = 0, \tag{A1i}$$

$$\left(i\frac{\partial}{\partial t} + d_{43}\right)\sigma_{43} + \Omega_a\sigma_{32}^* - \Omega_p^*\sigma_{41} - \Omega_c^*\sigma_{42} = 0, \tag{A1j}$$

where Γ_{ij} is the rate at which the population decays from the state $|j\rangle$ to the state $|i\rangle$, $d_{ij} = \Delta_i' - \Delta_j' + i\gamma_{ij}$ with $\Delta_i' = \Delta_i + \frac{\alpha_i}{2\hbar}|E_0|^2$, $\Delta_3 = \omega_p - (\omega_3 - \omega_1)$, $\Delta_2 = \omega_p - \omega_c - (\omega_2 - \omega_1)$, and $\Delta_4 = \omega_p - \omega_c + \omega_a - (\omega_4 - \omega_1)$ are the one-, two-, and three-photon detunings, respectively, $\gamma_{ij} \equiv (\Gamma_i + \Gamma_j)/2 + \gamma_{ij}^{\rm dph}$. Here $\Gamma_i = \sum_{E_i<E_j}\Gamma_{ij}$ and $\gamma_{ij}^{\rm col}$ denotes the dipole dephasing rate caused by atomic collisions.

[1] P. W. Anderson, Phys. Rev. **109**, 1492 (1958).
[2] B. Sacépé, T. Dubouchet, C. Chapelier, M. Sanquer, M. Ovadia, D. Shahar, M. Feigel'man, and L. Loffe, Nat. Phys. **7**, 239 (2011).
[3] I. S. Burmistrov, I. V. Gornyi, and A. D. Mirlin, Phys. Rev. Lett. **108**, 017002 (2012).
[4] J. Billy, V. Josse, Z. Zuo, A. Bernard, B. Hambrecht, P. Lugan, D. Clement, L. Sanchez-Palencia, P. Bouyer, and A. Aspect, Nature (London) **453**, 891 (2008).
[5] S. S. Kondov, W. R. McGehee, J. J. Zirbel, and B. DeMarco, Science **334**, 66 (2011).

[6] D. S. Wiersma, P. Bartolini, A. Lagendijk, and R. Righini, Nature (London) **390**, 671 (1997).
[7] A. A. Chabanov, M. Stoytchev, and A. Z. Genack, Nature (London) **404**, 850 (2000).
[8] J. Topolancik, B. Ilic, and F. Vollmer, Phys. Rev. Lett. **99**, 253901 (2007).
[9] T. Schwartz, G. Bartal, S. Fishman, and M. Segev, Nature (London) **446**, 52 (2007).
[10] Z. V. Vardeny and A. Nahata, Nat. Photonics **2**, 75 (2008).
[11] Y. Lahini, A. Avidan, F. Pozzi, M. Sorel, R. Morandotti, D. N. Christodoulides, and Y. Silberberg, Phys. Rev. Lett. **100**, 013906 (2008).
[12] H. Hu, A. Strybulevych, J. H. Page, S. E. Skipetrov, and B. A. van Tiggelen, Nat. Phys. **4**, 945 (2008).
[13] Y. Lahini, R. Pugatch, F. Pozzi, M. Sorel, R. Morandotti, N. Davidson, and Y. Silberberg, Phys. Rev. Lett. **103**, 013901 (2009).
[14] L. Levi, M. Rechtsman, B. Freedman, T. Schwartz, O. Manela, and M. Segev, Science **332**, 1541 (2011).
[15] G. Roati, C. D'Errico, L. Fallani, M. Fattori, C. Fort, M. Zaccanti, G. Modugno, M. Modugno, and M. Inguscio, Nature (London) **453**, 895 (2008).
[16] L. Fallani and M. Inguscio, Science **322**, 1480 (2008).
[17] U. Schneider, L. Hackermueller, S. Will, Th. Best, I. Bloch, T. A. Costi, R. W. Helmes, D. Rasch, and A. Rosch, Science **322**, 1520 (2008).
[18] B. Deissler, M. Zaccanti, G. Roati, C. D'Errico, M. Fattori, M. Modugno, and M. Inguscio, Nat. Phys. **6**, 354 (2010).
[19] L. Sanchez-Palencia, Nat. Phys. **6**, 328 (2010).
[20] M. Pasienski, D. Mckay, M. White, and B. DeMarco, Nat. Phys. **6**, 677 (2010).
[21] B. Horstmann, S. Durr, and T. Roscilde, Phys. Rev. Lett. **105**, 160402 (2010).
[22] L. P. Horwitz and Y. Ne'Tman, Proceedings of the 8th International Colloquium, Ann. Isr. Phys. Soc. **3**, 133 (1980).
[23] P. G. Harper, Proc. Phys. Soc. London A **68**, 874 (1955).
[24] M. Fleischhauer, A. Imamoglu, and J. P. Marangos, Rev. Mod. Phys. **77**, 633 (2005).
[25] J. Cheng and G. Huang, Phys. Rev. A **83**, 053847 (2011).
[26] H. Schmidt and A. Imamoğlu, Opt. Lett. **21**, 1936 (1996).
[27] G. Huang, L. Deng, and M. G. Payne, Phys. Rev. E **72**, 016617 (2005).
[28] D. A. Steck, rubidium 87 *D* line data, http://steck.us/alkalidata/.